Emergence of microfrequency comb via limit cycles in dissipatively coupled condensates

Seonghoon Kim,[1] Yuri G. Rubo,[2] Timothy C. H. Liew,[3] Sebastian Brodbeck,[4] Christian Schneider,[4] Sven Höfling,[4,5] and Hui Deng[6,*]

[1]*Department of Electrical Engineering and Computer Science, University of Michigan, Ann Arbor, Michigan 48109, USA*
[2]*Instituto de Energías Renovables, Universidad Nacional Autónoma de México, Temixco, Morelos 62580, Mexico*
[3]*Division of Physics and Applied Physics, School of Physical and Mathematical Sciences, Nanyang Technological University, 21 Nanyang Link, Singapore 637371, Singapore*
[4]*Technische Physik, Universität Würzburg, Am Hubland, Würzburg 97074, Germany*
[5]*SUPA, School of Physics and Astronomy, University of St Andrews, St Andrews KY16 9SS, United Kingdom*
[6]*Department of Physics, University of Michigan, 450 Church Street, Ann Arbor, Michigan 48109, USA*

(Received 26 February 2019; revised manuscript received 3 December 2019; accepted 4 February 2020; published 18 February 2020)

Self-sustained oscillations, limit cycles, are a fundamental phenomenon unique to nonlinear dynamic systems of high-dimensional phase space. They enable understanding of a wide range of cyclic processes in natural, social, and engineering systems. Here we show that limit cycles form in coupled polariton cavities following the breaking of Josephson coupling, leading to frequency-comb emission. The limit cycles and destruction of Josephson coupling both appear due to interplay between strong polariton-polariton interaction and a dissipative contribution to the cavity coupling. The resulting nonlinear dynamics of the condensates is characterized by asymmetric population distribution and nontrivial average phase difference between the two condensates, and by time-periodic modulation of their amplitudes and phases. The latter is manifested by coherent emission of new equidistant frequency components. The emission spectrum resembles that of a microfrequency comb, but originates from a fundamentally different mechanism than that of existing frequency combs. It allows nonresonant excitation with a power input much below the conventional semiconductor laser threshold. The comb line spacing is determined by the interaction and coupling strengths, and is adjustable up to multiterahertz frequency. The work establishes coupled polariton cavities as an experimental platform for rich nonlinear dynamic phenomena.

DOI: 10.1103/PhysRevB.101.085302

I. INTRODUCTION

In nonlinear dynamical systems, self-sustained oscillations, called limit cycles, may emerge from a stable fixed point when the system loses stability through Hopf bifurcation [1]. It is fundamentally different from periodic orbits in linear systems and requires a phase space of at least two dimensions. The oscillation becomes self-sustained; the oscillation frequency is set by the intrinsic dynamical properties of the system rather than initial conditions or the driving frequency. Studies of limit cycles have enabled understanding cyclic phenomena in nonlinear dynamical systems that are ubiquitous in our world, such as the beating of a heart [2], firing of nerve cells [3], chemical oscillations [4], predator-prey interactions [5], airplane propeller whirls [6], and relaxation oscillations in nonlinear electronic circuits [7]. The control of such intrinsic instabilities in nonlinear dynamic systems is not only crucial for many engineering systems but also might enable efficient neuromorphic computing [8,9] and the simulation of many-body phase transitions [10]. Here we demonstrate the emergence of limit cycles in a pair of coupled semiconductor exciton-polariton (EP) condensates, paving the way for creation and control of nonlinear dynamic phenomena in coupled, dissipative many-body systems.

Semiconductor microcavity EPs are formed by strong coupling between excitons and photons in high quality cavities [11]. They combine strong excitonic nonlinearity and robust long-range coherence, providing a fertile ground for complex nonlinear wave phenomena [12,13]. In single cavities, spin switching [14], critical slowing down [15], solitons [16], exceptional points [17], as well as multimode lasing and beating among modes [18] have all been observed. With recent developments in cavity engineering [19], we can now create multiple, coupled EP sites, where many phenomena that result from on-site interactions and coherent Josephson coupling have also been observed, such as Josephson oscillation [20], dynamical squeezing [21], and phase coupling [22]. While these phenomena share similarities to other coupled nonlinear matter-wave systems, microcavity EPs are special in that they are an intrinsically open, driven system. As a result, in addition to the coherent Josephson coupling, EP condensates may also couple dissipatively [23,24] when coupling modifies the radiation loss rates of the states. Such dissipative coupling has led to weak lasing in a one-dimensional EP lattice through supposedly a pitchfork bifurcation transition [25]. Richer phenomena that emerge in multidimensional phase space have also been predicted, including the formation of limit cycles through the Hopf bifurcation [24], which have not been reported in experiments to date.

Here, using a pair of tightly confined, single-mode EP cavities with controlled couplings, we experimentally demonstrate

*dengh@umich.edu

limit cycle oscillations, connected to the commonly observed stable EP lasing most likely via the Hopf bifurcation [26]. The limit cycle corresponds to a time-periodic modulation of the amplitudes and phases of the EP condensate. It is a uniquely nonlinear-dynamic phenomena and fundamentally different from population oscillation or beating between multiple stable eigenmodes of the system [18]. It is predicted to result in asymmetric population distribution, nontrivial phase relation between the two cavities, and most interestingly, the emergence of equidistant frequency components, in addition to and distinct from any of the static modes defined by the cavities [24,27]. We directly identify the limit cycles experimentally by new, additional frequency lines, with equidistant spacing, manifested in both spectral measurements and beating in the first-order coherence function. Moreover, we confirm three other key features predicted by the theory: asymmetric population distribution between the two coupled cavities, spontaneous current reflected in asymmetric emission in the Fourier space, and a nontrivial phase relation between the two cavities that is neither zero nor π.

This mechanism of frequency comb generation is fundamentally different from the widely studied ones using microresonators or quantum cascade lasers. The latter are based on resonantly driven cascaded four wave mixing, and the comb frequencies are determined by the cavity modes. The comblike EP emission due to limit cycles has a terahertz line spacing determined by the nonlinear interaction and coupling strengths and may enable a nonresonantly pumped, low-power source of microfrequency combs or terahertz waves.

II. TWO SITES CONDENSATION MODEL

To create the limit cycle state, we use a pair of EP condensates trapped close to each other. Photon tunneling between them leads to the Josephson coupling, resulting in the formation of bonding (B) and antibonding (A) states with split energies. Correspondingly, the radiation loss of the system is also modified, leading to different dissipation rates of the coupled states, which can be described as dissipative coupling between the condensates. The dissipation rate is higher (lower) when the two condensates are in phase (out of phase) and emission from the condensates interfere constructively (destructively) [23]. Consequently, the total coupling becomes non-Hermitian. The interplay between EP interactions and the non-Hermitian coupling between the condensates leads to rich nonlinear dynamic phenomena.

The dynamics of the polariton system is commonly described by the nonlinear Gross-Pitaevskii equations that includes pumping (P), loss (Γ), and polariton nonlinearities. To model the dynamics of our system, we include also both

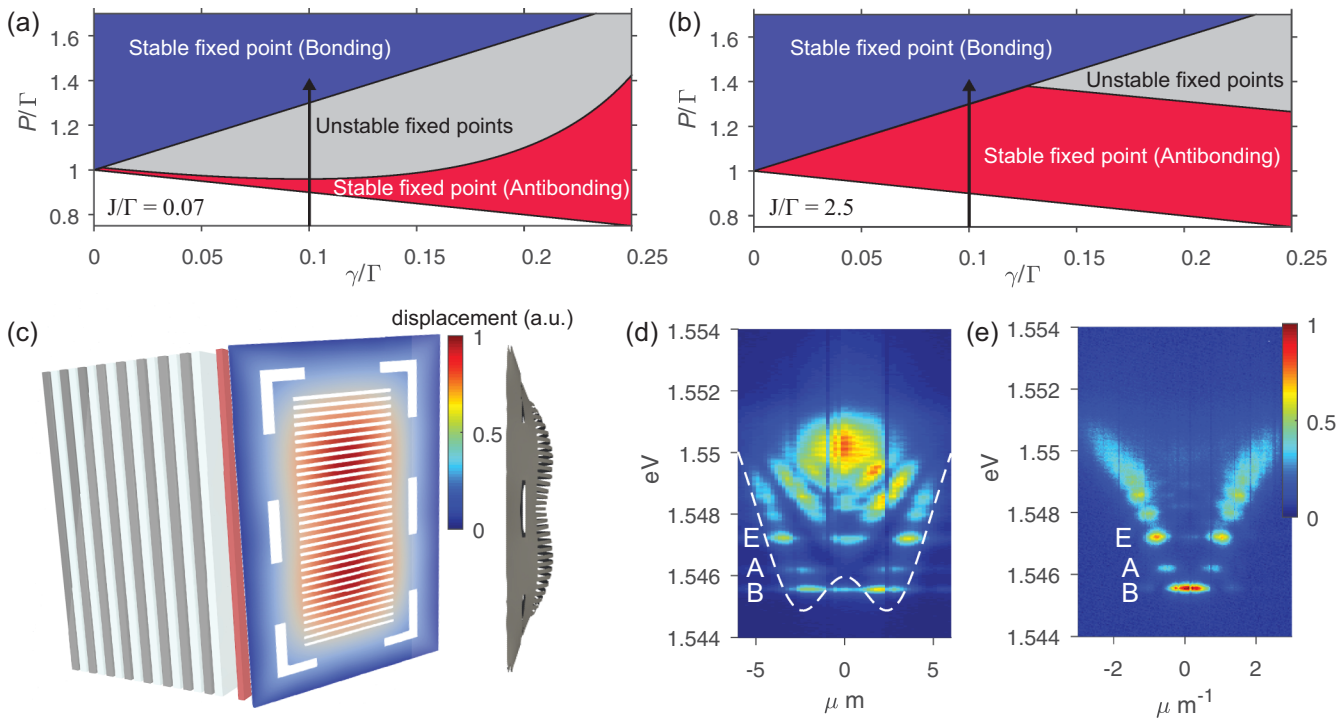

FIG. 1. Bifurcation diagram and the sample properties at low excitation powers. (a),(b) Bifurcation diagrams of Eq. (1) in $P-\gamma$ parameter space for $J/\Gamma = 0.07, 2.5$, respectively. For both diagrams, $\alpha/\Gamma = 0.25$, $\mu/\Gamma = 0.05$. A standard lasing threshold in the absence of dissipative coupling is at $P = \Gamma$. For certain values of $\gamma > 0$, thresholds for stable and unstable fixed-point solutions emerge as P increases, indicated by arrows for $\gamma/\Gamma = 0.1$. (c) A schematic of the sample structure with a bent SWG mirror. Bending of the SWG is simulated by COMSOL and shown both by the color map in the schematic view and in the side view. The bending is less where there are open slots in the tethering pattern and vice versa. (d), The real-space photoluminescence (PL) spectrum of the coupled polariton system showing the discrete polariton states at low excitation powers. Color represents PL intensity. The lowest-energy single-particle state of LPs is the bonding state (B state), while the first excited single-particle state of LPs is the antibonding state (A state). The next excited single-particle state of LPs is labeled as the E state. The white dashed line illustrates the potential due to the bending of the SWG shown in (c). (e) The corresponding Fourier space spectrum showing the B state at $k = 0$ and the A state at $k = \pm\pi/a$, where a is the distance between the two coupled sites.

coherent and dissipative coupling between the two sites, and obtain the following driven-dissipative coupled EP equation [24,28]:

$$\frac{d\psi_{L,R}}{dt} = \frac{1}{2}(p_{L,R}\psi_{L,R} - \gamma\psi_{R,L} - \mu|\psi_{L,R}|^2\psi_{L,R}) - \frac{i}{2}(2\omega_{L,R}\psi_{L,R} - J\psi_{R,L} + \alpha|\psi_{L,R}|^2\psi_{L,R}). \quad (1)$$

Here $\psi_{L,R}$ is the order parameter of the condensate in the left (L) and the right (R) site, respectively; $\omega_{L,R}$ are the frequencies of the uncoupled cavity modes; $p_{L,R} = P_{L,R} - \Gamma$ where $P_{L,R}$ is the incoherent pump strength acting on the L, R site and Γ is the cavity decay rate; γ is the dissipative coupling strength; μ is the gain saturation parameter; J is the Josephson coupling strength; and α is the on-site interaction strength.

Two examples of phase diagrams based on Eq. (1) are shown in Figs. 1(a) and 1(b) as a function of the pump rate P and dissipative coupling rate γ, for fixed $J/\Gamma = 0.07$ and 2.5, respectively. With increasing pump rate P, the system transitions from a thermal state to two possible types of stable lasing states: weak lasing in an EP state with the lowest decay rate and lasing in an EP state with the lowest energy—the bonding state of the coupled EP system. Both are fixed-point solutions of the coupled system. With a sufficiently large dissipative coupling strength γ, limit cycle solutions, or comb states, can exist between the two stable fixed points. We note that to produce the limit cycles, a large on-site interaction $\alpha \gg \mu$ is necessary, which can be realized with tight confinement of the EPs [29]. As shown in the figures, for larger J/Γ [Fig. 1(b)], the unstable fixed-point domain in the parameter space becomes small and requires large dissipative coupling γ, making it harder to realize experimentally. However, decreasing J, coherent coupling between the site, would often lead to a decrease in γ, the dissipative coupling between the two sites. For fixed J and γ, a relatively large Γ may facilitate the creation of the limit cycle state, but it also needs to be sufficiently low to allow stimulated scattering and formation of coherent condensates. Therefore optimal values of Γ, J, and α exist to achieve a comb state.

The limit cycles, formed at the intermediate pumping, are typically highly anharmonic, as it is shown in Figs. 2(a)–2(c), for the symmetric case with $p_L = p_R = p$ and $\omega_L = \omega_R = 0$. For small pumping, the limit cycle (LC) is formed in a symmetry broken state, with different average occupations of the L and R sites; see Fig. 2(a). In this case, the system chooses randomly between two possible LC states. There is a critical pumping p_s, however, where the symmetry is restored. The period of LC is doubled at this transition. For the parameters in Fig. 2, $p_s \approx 0.76\Gamma$. Far from the $p = p_s$ point, the LC dynamics results in only one or two strong spectral lines, while close to this point there are several pronounced lines.

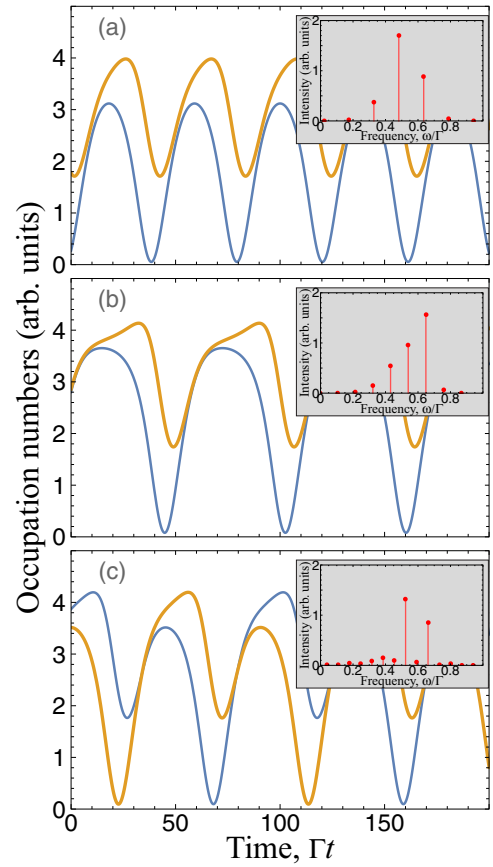

FIG. 2. Showing the time dependence of the site occupation numbers in the limit cycle regime, for $J/\Gamma = \gamma/\Gamma = 0.15$, $\alpha/\mu = 5$, and pumpings (a) $p = 0.7\Gamma$, (b) $p = 0.76\Gamma$, (c) $p = 0.8\Gamma$. The positions and intensities of corresponding spectral lines are shown in the insets.

III. EXPERIMENTAL SYSTEM

The GaAs-based microcavity device we use is illustrated in Fig. 1(c). The top mirror consists of a $Al_{0.15}Ga_{0.85}As$ subwavelength grating (SWG) suspended over a short distributed Bragg reflector (DBR) of 2.5 pairs of $Al_{0.15}Ga_{0.85}As/AlAs$. The bottom mirror consists of a DBR of 30 pairs of $Al_{0.15}Ga_{0.85}As/AlAs$ layers. The $\lambda/2$ AlAs cavity has three stacks of four GaAs quantum wells placed at the electric-field maxima. The Rabi splitting of 12 meV at 5 K was measured from the uncoupled single site. The properties of single SWG-DBR EP systems and polariton lasing in this system have been studied in detail before [29,30].

The use of the SWG mirror enables the creation of confined and coupled EPs. Lateral confinement of the EPs and full discretization of the EP modes are created and controlled by the lateral size of the SWG mirror [30], while multiple, coupled EP sites are created by controlling the placements of the grating bars and the tethering pattern surrounding the SWG [31]. The tethering pattern controls the strain release when the sacrificial layer is removed and in turn controls the bending of the individual grating bars, as shown by simulations using COMSOL Multiphysics [Fig. 1(c)]. The bending of the SWG directly modulates the cavity length and thus the exciton-cavity detuning, through which we form a trapping potential for EPs. Controlling the location and shape of the tethering patterns, therefore, controls both the height and width of the potential barrier between two sites. This tunability provides us control over both the on-site interaction [29] and intersite coupling [31] of the EPs. Specifically, the length of the grating bar determines the size of the polariton mode in the single site and therefore controls the on-site

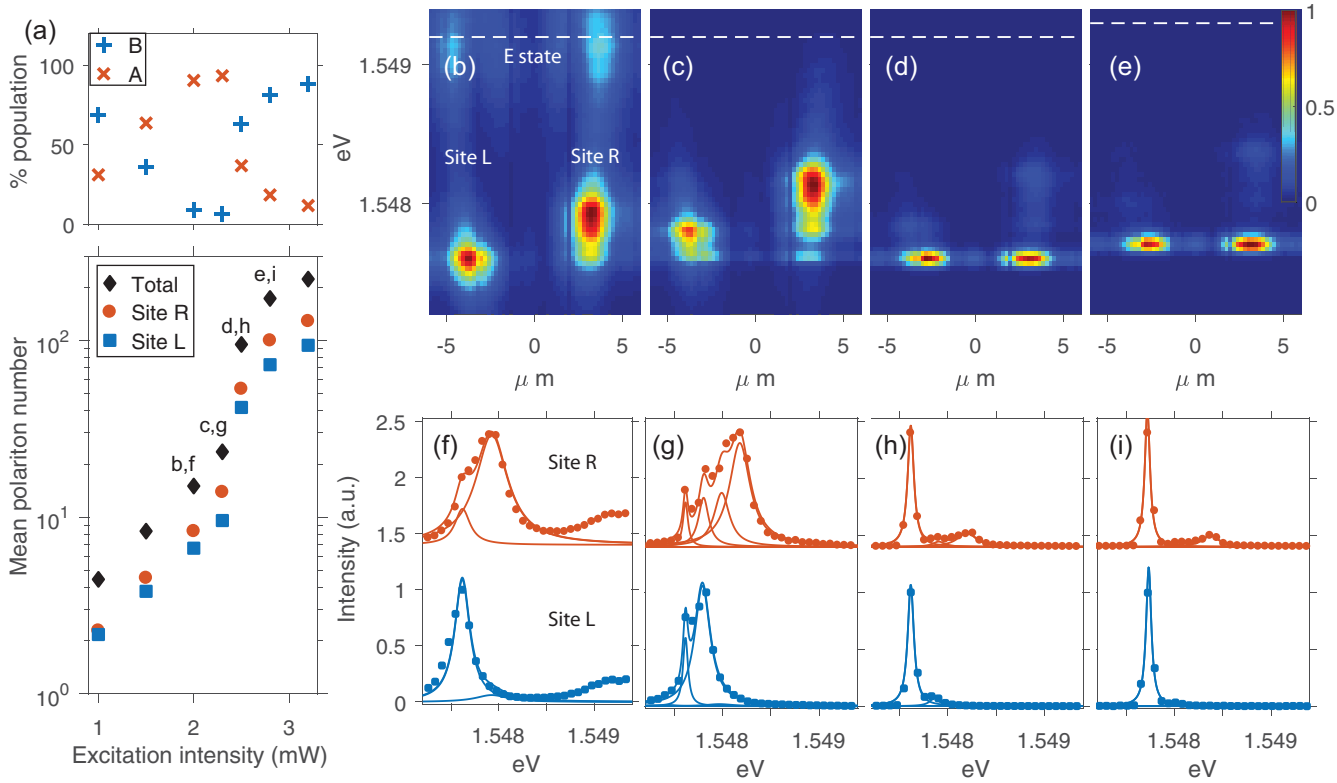

FIG. 3. Excitation power dependence of the intensity and real-space spectra of the polariton PL near the A and B states. (a) Bottom: Mean polariton number of the A and B states vs the excitation power for the L site (blue square), R site (red circle), and the sum of the L and R sites (black diamond). It shows clearly a threshold behavior and degenerate occupation at each site. Top: Relative fraction of the B state (blue plus) and A state (red cross) population vs the excitation power, showing switching of the dominant state upon transitions to stable weak lasing near A state followed by the limit cycles, and to stable lasing in the B state. (b)–(e) The real-space spectra at four different excitation powers as marked in (a), showing the transition from weak lasing, to limited cycles, toward B state lasing. The white dashed line marks the E state—the next lowest energy state above the B and A states. (f)–(i) Spectrum of each site obtained from (b) to (e), respectively. The solid lines are fits by equidistant Lorentzians.

interaction strengths. The center-to-center distance controls the Josephson and dissipative coupling strengths.

In all our experiments, the microcavity sample is kept at 5 K in a closed-cycle cryostat and excited by a continuous-wave Ti:sapphire laser chopped with electo-optic modulator at 5 kHz with 5% duty cycle. The pump spot is focused on the center of the device with a diameter of 2 μm.

Figures 1(d) and 1(e) show the real-space and Fourier-space photoluminescence (PL) spectra of the EPs at low pump powers. The states are discretized due to tight confinement, which also enhances the on-site interaction to the order of 10 μeV due to increased EP density [29]. Bonding (B) and antibonding (A) states are formed due to Josephson coupling. Their separation gives the coupling strength $J = 0.5$ meV. The Josephson coupling decreases as the pump power increases, because the pump is located at the center of the device and creates a local carrier population that adds to the potential barrier between the two sites (see Supplemental Material Fig. S1 for the narrowing of energy separation between the bonding and antibonding states [32]). The distance between the two minima of the effective potential is 6.4 μm, corresponding to the separation of the two cavity sites. The next lowest energy state, labeled as state E in Fig. 1, is formed from the first excited state of each uncoupled site. It is 1.4 meV above state A, far separated from the lasing frequencies of the stable fixed points or limit cycles.

IV. SPECTRAL SIGNATURES

We first observe signatures of the limit-cycle state and estimate the dissipative coupling rate through the power dependence of the spectral and spatial distributions of the emission. The power dependence of the real-space spectra is shown in Fig. 3. The PL spectrum at the low power [Figs. 1(d) and 1(e)] shows clearly the eigenstates of the system, with the three lowest ones the B state, A state, and E state. The bonding state B initially has a larger population than the state A, because the pump spot is placed at the center of the device and prefers the B state. As the pump power increases, the antibonding state A becomes more populated than state B [Figs. 3(a), 3(b), and 3(f)]. This suggests the onset of weak lasing at $P = \Gamma - \gamma$ in the state with a lower decay rate [23]. The apparent asymmetry between the two sites, manifested in different intensities and different numbers of limit cycle lines visible from each site, is also consistent with the symmetry breaking in the weak lasing regime [23,24]. With increasing power, limit-cycle oscillations appear, leading to the appearance of new frequency components [Figs. 3(c), 3(d), 3(g),

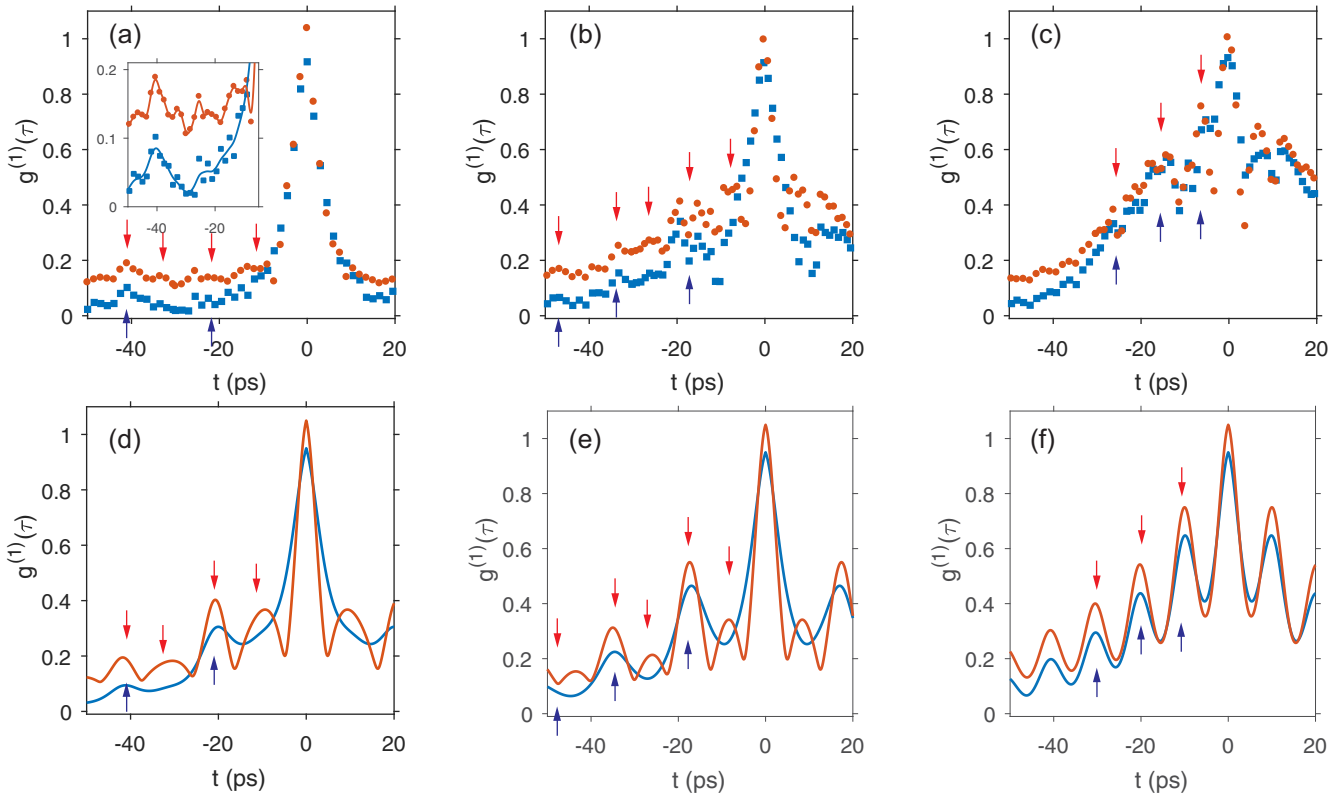

FIG. 4. Experimental (a)–(c) and theoretical (d)–(f) $g^{(1)}(\tau)$ for three different excitation powers, corresponding to Figs. 3(c)–3(e), respectively. Red dots are shifted vertically by 0.1 for better visibility. The inset shows a zoom in of the revival peaks in (a). The lines are guides to the eye. The blue and red arrows indicate experimentally measured beating peaks and corresponding peaks in simulations for site L and R, respectively. The site with more frequency lines has more revival peaks and narrower $g^{(1)}(\tau)$ linewidths at $\tau = 0$. The simulated $g^{(1)}(\tau)$ is multiplied by an exponential decay with decay times of 20, 25, 30 ps respectively.

and 3(h)]. We fit the spectrum of each site to equidistant Lorentzian lines. Above the bifurcation threshold, up to four equidistant lines are resolved for the right site R (red), and up to three for the left site L (blue), with fitted line spacing of 0.19 and 0.27 meV, respectively, which should correspond approximately to the dissipative coupling rate [24]. We note that all these frequency lines are near the original A and B state and far below the E state. At high pump powers, the PL eventually becomes dominated by the B state and other frequency components become insignificant, showing the system is transitionary toward the single-mode B state lasing [Figs. 3(e) and 3(h)]. (See the Supplemental Materials for the case when single-mode B state lasing is reached in the system [32].) This second transition takes place at $P = \Gamma + 3\gamma$. This sequence of transitions agrees with the dissipative coupling modeled by Eq. (1) and allows us to estimate the dissipative coupling rate for our system as $\gamma = 0.055\ \mathrm{ps}^{-1}$, or 0.23 meV (see the Appendix for details). It is consistent with the comb spacing obtained from the spectral fit.

V. COHERENCE REVIVAL

To verify the uniformity of the mode spacing and phase coherence between the multiple frequency lines, we measure the temporal first-order coherence $g^{(1)}(\tau)$ using a Michelson interferometer. As shown in Fig. 4, $g^{(1)}(\tau)$ features a main central peak that decays over a few picoseconds, corresponding to the full spread of the multiple frequency lines. At larger τ, instead of a smooth decay, multiple small peaks are apparent. Such coherence revivals confirm that the emission consists of multiple equidistant, coherent frequency lines. On the R site, where four frequency components are present, a larger number and more distinct revival peaks are observed compared to the L site. At low power, a clear revival peak is measured at 40 ps for both sites, but other revival peaks are less well resolved due to the low coherence time [Fig. 4(a)]. As the populations in the two sites grow, the coherence time becomes longer, and the revival peaks become more apparent [Fig. 4(b)]. At higher powers [Fig. 4(c)], the number of revival peaks and the complexity in $g^{(1)}(\tau)$ decrease, suggesting the reduction of frequency components as the system evolves toward the stable fixed point of bonding state lasing. We compare the experimental $g^{(1)}(\tau)$ with computed results $g^{(1)}_{\mathrm{sim}}(\tau) = g^{(1)}_0(\tau)\exp(-\tau/\tau_{\mathrm{decay}})$, where $g^{(1)}_0(\tau)$ is based on Eq. (1) (see the Appendix for parameter values of the model) and τ_{delay} corresponds to the decay time of $g^{(1)}$ due to the Langevin noise. Values of τ_{decay} are obtained from the decay time of the envelope of the measured $g^{(1)}(\tau)$. The results are shown in Figs. 4(d)–4(f), which qualitatively capture the main features of the measured coherence revivals. The corresponding dissipative coupling rate used in the simulation is $0.077\ \mathrm{ps}^{-1}$, or 0.32 meV, which is reasonable compared to the dissipative coupling rate of 0.23 meV estimated from transition thresholds in Sec. IV.

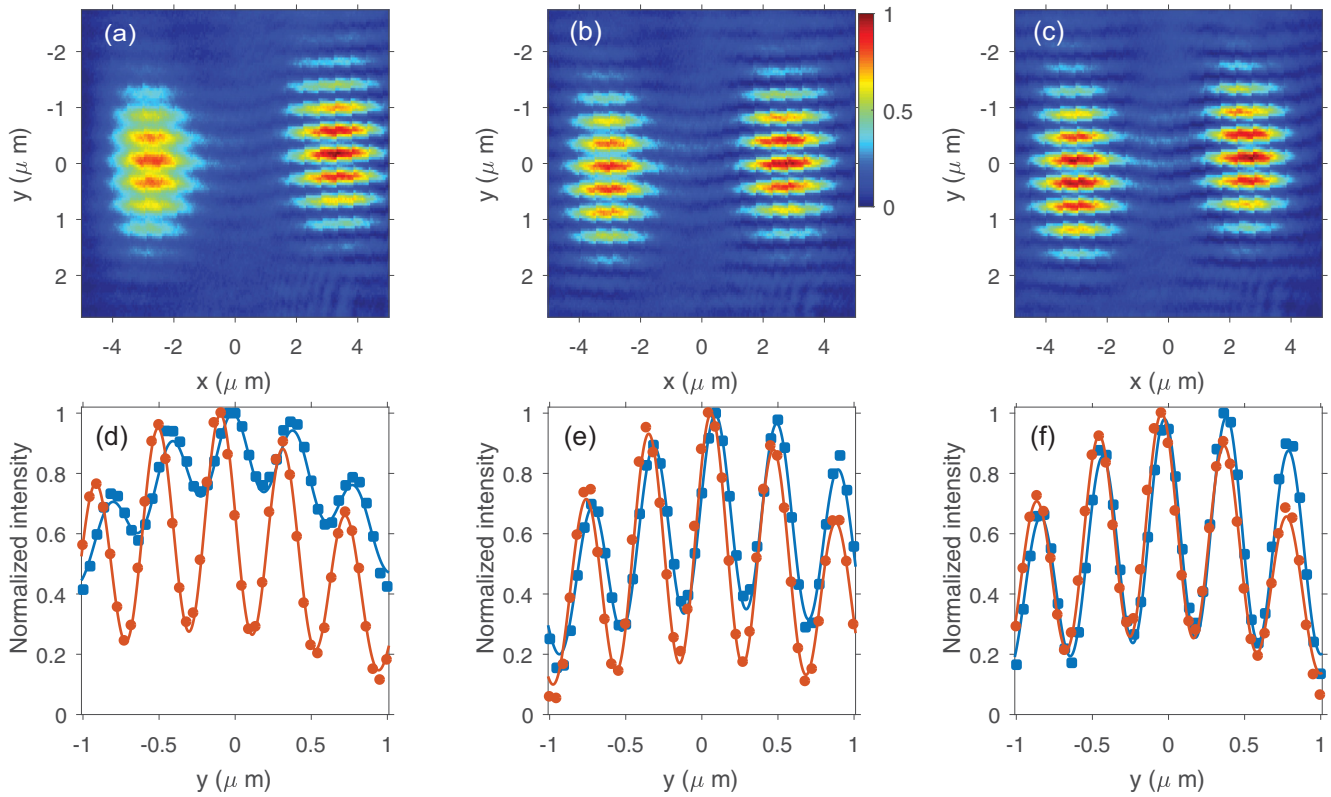

FIG. 5. Relative phase measurement between L and R sites at excitation powers of 2 mW (a),(d), 2.3 mW (b),(e), and 2.5 mW (c),(f). (a)–(c) Interference images from interfering both sites to a magnified single site. (d)–(f) Interference fringes for each site obtained from (a)–(c) along $x = \pm 3$ μm (dots). The solid lines are fits as described in the text. From the fit, we obtain the relative phase difference of $0.51 \pm 0.08\,\pi$, $0.21 \pm 0.06\,\pi$, and $0.15 \pm 0.04\,\pi$ respectively.

VI. RELATIVE PHASE

Last, a hallmark of the limit-cycle state is a nontrivial relative phase ϕ between the two sites. The dissipative coupling alone favors an out-of-phase relationship between the two sites with $\phi = \pi$. At the same time, on-site interaction changes the instantaneous frequency of each site. Interplay between these two results in a nontrivial phase $\phi \neq 0$ or π between the two sites when stable limit-cycle oscillations are formed.

To measure the relative phase ϕ, we use the emission from one of the sites as a phase reference to determine the relative phase between the two sites [33], as the absolute phase of the polariton condensate is different for every experimental realization. We use a Mach-Zehnder interferometer and magnify the image from one arm by a factor of 6 compared to the other arm. For two spatial modes of 2 μm in diameter separated by 7 μm, magnification of about 4.5 is needed in order for the single site to interfere with the entire system. Our magnification ensures that the two sites overlap with the center of the single site where the phase is uniform. Examples are shown in Fig. 5. We then fit the interference pattern in each site to $I_{L,R}(x) = I_{L,R}(x)[1 + |g^{(1)}_{L,R}|\cos(k_x x + \phi_{L,R})]$, where $I(x)$ is the Gaussian intensity profile and k_x is the spatial frequency of the fringe pattern due to the angle between two interfering beams. The relative phase is calculated as $\phi = |\phi_L - \phi_R|$.

As shown in Fig. 5, we obtain $\phi = 0.51 \pm 0.08\,\pi$ when the multiple frequency lines appear [Figs. 5(a) and 5(d)]. When the B state brightens up at high powers, the relative phase changes to $\phi = 0.21 \pm 0.06\,\pi$ [Figs. 5(b) and 5(e)] and $0.15 \pm 0.04\,\pi$ [Figs. 5(c) and 5(f)], converging toward an in-phase relation for single-mode B state lasing. The above nontrivial phase relationship is also evidenced by the shift of the $k = 0$ peak in the power dependence of the k-space PL spectra as shown in the Supplemental Material [32].

VII. DISCUSSION

The above experimental observations consistently show the formation of limit cycle oscillations in dissipatively coupled polariton condensates. The direct manifestation is the emergence of new, additional frequency lines in the spectra. Although the equidistant lines are not fully spectrally separate, their existence is unmistakable. Their mutual coherence is confirmed by $g^{(1)}$ measurements.

Three other features all support this interpretation. The asymmetric population distribution between the two coupled cavities, corroborated by spontaneous current reflected in asymmetric emission in the Fourier space, are both incompatible with stable emission from condensates formed in A or B states. The bonding and antibonding states both have symmetric population distribution between the two sites, in both real space and k space, which is clearly shown in our data, both at low pump powers in the linear regime, and at very high powers when the system converges to stable bonding-state

lasing corresponding to a stable fixed point. Only in the limit cycle regime, where the new frequency lines appear, is the symmetry broken between the two sites. Such symmetry breaking, especially in k space, is an important characteristic of the limit cycle phase.

Similarly, the nontrivial phase relation between the two cavities is also unusual and quite unique to the limit cycle regime. The two sites are exactly in phase in the bonding state, and exactly out of phase π in the antibonding state. In phase-locked multiple mode condensate, the relative phase among different modes is also zero. It is only due to dissipative coupling, which introduces dynamic instability between the bonding and antibonding state, that a limit cycle forms with a relative phase neither zero nor π between the two sites. Such a nontrivial phase relation in a coherent condensate has not been predicted by other mechanisms, and has been considered a telltale property of the limit cycles.

VIII. CONCLUSION

In conclusion, we demonstrate a limit cycle transition in a pair of dissipatively coupled nonlinear polariton condensates. Signatures of the limit cycle transition are measured, including the generation of equidistant new frequency components, corresponding coherence revivals in $g^{(1)}(\tau)$, asymmetric distribution in both real and Fourier space, and a nontrivial relative phase that is neither zero nor π. These signatures are distinct from those of multistate lasing, four-wave mixing among the static eigenmodes of the polariton system, or weak lasing.

Our results also allow us to estimate the dissipative coupling rate. From the excitation dependence of the transition, we infer a dissipative coupling rate about one-tenth of the cavity decay rate, or $\gamma \sim 0.23$ meV, consistent with the comb line spacing of 0.19–0.27 meV as well as the value of 0.32 meV based on simulation of the coherence revival features in $g^{(1)}(\tau)$.

The multiple, equidistant lines resulting from the limit cycle oscillation resemble a microfrequency comb. Such a comb allows nonresonant or electrical excitations [34] with very low input power, as it takes place near the polariton lasing threshold without electronic population inversion. Future work to modify the quality factor and interaction strength of the microcavities may result in narrower linewidth of individual comb lines and greater line spacing. Scaling up the system to a lattice of condensate may provide a platform for efficient neuromorphic computing [8,9] and simulation of many-body phase transitions [10].

Note added. After the submission of this work, limit cycle in a pair of coupled vertical cavity surface emitting lasers was reported [35].

ACKNOWLEDGMENTS

S.K. and H.D. acknowledge the support by the National Science Foundation (NSF) under Award No. DMR 1150593 and the Air Force Office of Scientific Research under Award No. FA9550-15-1-0240. Y.G.R. acknowledges the support from CONACYT (Mexico) Grant No. 251808 and from PAPIIT-UNAM Grant No. IN106320. T.L. was supported by the Ministry of Education (Singapore) Grant No. 2017-T2-1-001. C.S., S.B., and S.H. acknowledge the support by State of Bavaria and the Deutsche Forschungsgemeinschaft (DFG) within Project No. SCHN11376 3-1. The fabrication of the SWG microcavities was performed in the Lurie Nanofabrication Facility (LNF) at Michigan, which is part of the NSF NNIN network.

APPENDIX: NUMERICAL SIMULATION

We numerically solved Eq. (1) using a fourth-order Adams-Bashforth-Moulton predictor-corrector method with small initial populations in both sites. Note that the initial condition does not affect the final state which converges to the limit-cycle solution. To account for the effect of noise, we multiplied exponential decay functions to the simulated $g^{(1)}(\tau)$. The parameters used for Figs. 3(d)–3(f) were $\Gamma = 0.5\ \mathrm{ps}^{-1}$, $\gamma = 0.077\ \mathrm{ps}^{-1}$, $\omega = 0$, $J = 0.077\ \mathrm{ps}^{-1}$, $\alpha = 1.15\ \mathrm{ps}^{-1}$, and $\mu = 0.015\ \mathrm{ps}^{-1}$. It is important to note that α used in the simulation is the polariton interaction strength multiplied by the polariton population. Considering the polariton population obtained experimentally, one requires the polariton interaction strength to be about 10 μeV, which is in agreement with previous reports in GaAs polariton systems. We changed the pumping strength P to account for the strength of the excitation power assuming other parameters do not change significantly above the lasing threshold. We used $P = 0.524,\ 0.548,\ 0.627\ \mathrm{ps}^{-1}$ respectively. We also gave a 1% difference in pumping strength between two sites to account for the asymmetry in experiments.

The dissipative coupling strength can be estimated by the observed thresholds. It is convenient to express Eq. (1) based on a pseudospin vector defined as $\mathbf{S} = \frac{1}{2}(\mathbf{\Psi}^\dagger \cdot \boldsymbol{\sigma} \cdot \mathbf{\Psi})$, where $\mathbf{\Psi} = (\psi_1, \psi_2)^T$ and $\boldsymbol{\sigma}$ is the Pauli vector,

$$\begin{aligned}
\frac{dS_x}{dt} &= (p - \mu S)S_x - \gamma S - \alpha S_z S_y, \\
\frac{dS_y}{dt} &= (p - \mu S)S_y + JS_z + \alpha S_z S_x, \\
\frac{dS_z}{dt} &= (p - 2\mu S)S_z - JS_y, \\
\frac{dS}{dt} &= (p - \mu S)S - \mu S_z^2 - \gamma S_x,
\end{aligned}$$

where $S_x = \frac{1}{2}(\psi_2^*\psi_1 + \psi_1^*\psi_2)$, $S_y = \frac{i}{2}(\psi_2^*\psi_1 - \psi_1^*\psi_2)$, $S_z = \frac{1}{2}(|\psi_1|^2 - |\psi_2|^2)$, $S = \frac{1}{2}(|\psi_1|^2 + |\psi_2|^2)$. Then the nontrivial fixed point A state becomes stable when $p = -\gamma$ and $S_x = -S$, $S_y = S_z = 0$, $S = (\gamma + p)/\mu$. This happened at the pump power of about 2 mW in the experiment [Fig. 3(b)]. The threshold for the stable fixed point B state is when $p = 3\gamma$ and $S_x = S$. This corresponds to the pump power of about 3 mW when the system stabilized to the B state with weak satellite peaks [Fig. 3(e)]. Assuming $\Gamma = 0.5\ \mathrm{ps}^{-1}$ and P is a linear function of pump power, the estimated dissipative coupling strength is about $0.055\ \mathrm{ps}^{-1}$ which is reasonable considering the value we used for the simulation.

[1] S. H. Strogatz, *Nonlinear Dynamics and Chaos: With Applications to Physics, Biology, Chemistry, and Engineering*, 2nd ed. (Westview, Boulder, CO, 2015).

[2] A. Babloyantz and A. Destexhe, Is the normal heart a periodic oscillator?, Biol. Cybern. **58**, 203 (1988).

[3] J. Rinzel and G. B. Ermentrout, Analysis of neural excitability and oscillations, in *Methods in Neuronal Modeling: From Synapses to Networks*, 2nd ed., edited by C. Koch and I. Segev (MIT Press, Cambridge, MA, 1998), pp. 251–291.

[4] R. J. Field and R. M. Noyes, Oscillations in chemical systems. IV. Limit cycle behavior in a model of a real chemical reaction, J. Chem. Phys. **60**, 1877 (1974).

[5] R. M. May, Limit cycles in predator-prey communities, Science **177**, 900 (1972).

[6] J. V. Carroll and R. K. Mehra, Bifurcation Analysis of Nonlinear Aircraft Dynamics, J. Guid. Control. Dyn. **5**, 529 (1982).

[7] B. van der Pol, Forced oscillations in a circuit with non-linear resistance. (Reception with reactive triode), Philos. Mag. (1798-1977) **3**, 65 (1927).

[8] N. Bertschinger and T. Natschlger, Real-Time Computation at the Edge of Chaos in Recurrent Neural Networks, Neural Comput. **16**, 1413 (2004).

[9] A. Opala, S. Ghosh, T. C. H. Liew, and M. Matuszewski, Neuromorphic Computing in Ginzburg-Landau Lattice Systems, Phys. Rev. Appl. **11**, 064029 (2019).

[10] M. Foss-Feig, P. Niroula, J. T. Young, M. Hafezi, A. V. Gorshkov, R. M. Wilson, and M. F. Maghrebi, Emergent equilibrium in many-body optical bistability, Phys. Rev. A **95**, 043826 (2017).

[11] C. Weisbuch, M. Nishioka, A. Ishikawa, and Y. Arakawa, Observation of the Coupled Exciton-Photon Mode Splitting in a Semiconductor Quantum Microcavity, Phys. Rev. Lett. **69**, 3314 (1992).

[12] H. Deng, H. Haug, and Y. Yamamoto, Exciton-polariton Bose-Einstein condensation, Rev. Mod. Phys. **82**, 1489 (2010).

[13] I. Carusotto and C. Ciuti, Quantum fluids of light, Rev. Mod. Phys. **85**, 299 (2013).

[14] A. Amo, T. C. H. Liew, C. Adrados, R. Houdr, E. Giacobino, A. V. Kavokin, and A. Bramati, Excitonpolariton spin switches, Nat. Photon. **4**, 361 (2010).

[15] T. Fink, A. Schade, S. Hfling, C. Schneider, and A. Imamoglu, Signatures of a dissipative phase transition in photon correlation measurements, Nat. Phys. **14**, 365 (2018).

[16] M. Sich, D. N. Krizhanovskii, M. S. Skolnick, A. V. Gorbach, R. Hartley, D. V. Skryabin, E. A. Cerda-Mndez, K. Biermann, R. Hey, and P. V. Santos, Observation of bright polariton solitons in a semiconductor microcavity, Nat. Photon. **6**, 50 (2012).

[17] T. Gao, E. Estrecho, K. Y. Bliokh, T. C. H. Liew, M. D. Fraser, S. Brodbeck, M. Kamp, C. Schneider, S. Hfling, Y. Yamamoto, F. Nori, Y. S. Kivshar, A. G. Truscott, R. G. Dall, and E. A. Ostrovskaya, Observation of non-Hermitian degeneracies in a chaotic exciton-polariton billiard, Nature (London) **526**, 554 (2015).

[18] G. Tosi, G. Christmann, N. G. Berloff, P. Tsotsis, T. Gao, Z. Hatzopoulos, P. G. Savvidis, and J. J. Baumberg, Sculpting oscillators with light within a nonlinear quantum fluid, Nat. Phys. **8**, 190 (2012).

[19] C. Schneider, K. Winkler, M. D. Fraser, M. Kamp, Y. Yamamoto, E. A. Ostrovskaya, and S. Höfling, Exciton-polariton trapping and potential landscape engineering, Rep. Prog. Phys. **80**, 016503 (2017).

[20] M. Abbarchi, A. Amo, V. G. Sala, D. D. Solnyshkov, H. Flayac, L. Ferrier, I. Sagnes, E. Galopin, A. Lematre, G. Malpuech, and J. Bloch, Macroscopic quantum self-trapping and Josephson oscillations of exciton polaritons, Nat. Phys. **9**, 275 (2013).

[21] A. F. Adiyatullin, M. D. Anderson, H. Flayac, M. T. Portella-Oberli, F. Jabeen, C. Ouellet-Plamondon, G. C. Sallen, and B. Deveaud, Periodic squeezing in a polariton Josephson junction, Nat. Commun. **8**, 1329 (2017).

[22] H. Ohadi, R. L. Gregory, T. Freegarde, Y. G. Rubo, A. V. Kavokin, N. G. Berloff, and P. G. Lagoudakis, Nontrivial Phase Coupling in Polariton Multiplets, Phys. Rev. X **6**, 031032 (2016).

[23] I. L. Aleiner, B. L. Altshuler, and Y. G. Rubo, Radiative coupling and weak lasing of exciton-polariton condensates, Phys. Rev. B **85**, 121301(R) (2012).

[24] K. Rayanov, B. L. Altshuler, Y. G. Rubo, and S. Flach, Frequency Combs with Weakly Lasing Exciton-Polariton Condensates, Phys. Rev. Lett. **114**, 193901 (2015).

[25] L. Zhang, W. Xie, J. Wang, A. Poddubny, J. Lu, Y. Wang, J. Gu, W. Liu, D. Xu, X. Shen, Y. G. Rubo, B. L. Altshuler, A. V. Kavokin, and Z. Chen, Weak lasing in one-dimensional polariton superlattices, Proc. Natl. Acad. Sci. USA **112**, E1516 (2015).

[26] To conclusively show Hopf bifurcation, one will need to show, for example, that the limit cycle amplitude scales as a square root of the distance to the bifurcation point, which is infeasible in our experiment.

[27] S. Khan and H. E. Türeci, Frequency Combs in a Lumped-Element Josephson-Junction Circuit, Phys. Rev. Lett. **120**, 153601 (2018).

[28] H. Ohadi, A. Dreismann, Y. G. Rubo, F. Pinsker, Y. del Valle-Inclan Redondo, S. I. Tsintzos, Z. Hatzopoulos, P. G. Savvidis, and J. J. Baumberg, Spontaneous Spin Bifurcations and Ferromagnetic Phase Transitions in a Spinor Exciton-Polariton Condensate, Phys. Rev. X **5**, 031002 (2015).

[29] S. Kim, B. Zhang, Z. Wang, J. Fischer, S. Brodbeck, M. Kamp, C. Schneider, S. Höfling, and H. Deng, Coherent Polariton Laser, Phys. Rev. X **6**, 011026 (2016).

[30] B. Zhang, Z. Wang, S. Brodbeck, C. Schneider, M. Kamp, S. Höfling, and H. Deng, Zero-dimensional polariton laser in a subwavelength grating-based vertical microcavity, Light: Sci. Appl. **3**, e135 (2014).

[31] B. Zhang, S. Brodbeck, Z. Wang, M. Kamp, C. Schneider, S. Höfling, and H. Deng, Coupling polariton quantum boxes in sub-wavelength grating microcavities, Appl. Phys. Lett. **106**, 051104 (2015).

[32] See Supplemental Material at http://link.aps.org/supplemental/10.1103/PhysRevB.101.085302 for relative phase evolution from k-space spectra, theoretical Fourier transform spectra of the first-order coherence function, and an example of transition from limit cycle to stable single-mode lasing.

[33] F. Manni, K. G. Lagoudakis, T. C. H. Liew, R. André, and B. Deveaud-Plédran, Spontaneous Pattern Formation in a Polariton Condensate, Phys. Rev. Lett. **107**, 106401 (2011).

[34] H. Suchomel, S. Klembt, T. H. Harder, M. Klaas, O. A. Egorov, K. Winkler, M. Emmerling, S. Hoefling, and C. Schneider, An Electrically Pumped Polaritonic Lattice Simulator, Phys. Rev. Lett. **121**, 257402 (2018).

[35] M. Marconi, F. Raineri, A. Levenson, A. M. Yacomotti, J. Javaloyes, S. H. Pan, A. E. Amili, and Y. Fainman, Mesoscopic limit cycles in coupled nanolasers, arXiv:1911.10830.